

Seeing the Turnover in the Brightness Distribution of Complex Gamma Ray Bursts

Boris Stern^{1,2}, Juri Poutanen^{2,3}, Roland Svensson²

ABSTRACT

We observe strong correlations between the temporal properties of GRBs and their apparent brightness. The strongest effect is the difference between the brightness distributions of simple bursts (dominated by a single smooth pulse) and complex bursts (consisting of overlapping pulses). The latter has a break at a peak brightness $\sim 1.5 \text{ ph cm}^{-2} \text{ s}^{-1}$. The peak count rates of complex bursts systematically exceed those of simple bursts by a factor of ~ 2 , the effect has significance level of $\sim 10^{-7}$. We also observe brightness dependent variations in the shape of the average time profile (ATP) of GRBs: the decaying slope of the ATP shows time dilation when comparing bright and dim bursts while the rising slope hardly changes. Both slopes of the ATP are deformed for weak bursts as compared to strong bursts. The interpretation of these effects is simple: a complex burst where a number of independent pulses overlap in time appears intrinsically stronger than a simple burst. Then the BATSE sample of complex bursts covers larger redshifts where some cosmological factor causes the break in the brightness distribution. The break seems too sharp to be explained with a non-evolving source population. We suggest that the break corresponds to the peak in the star formation rate at $z \sim 1.5$ which was revealed recently by the *Hubble Space Telescope* observations.

Subject headings: Gamma-ray bursts – Methods: data analysis

1. Introduction

Do the temporal properties of GRBs have systematic trends dependent on brightness? The trend which has been the most intensively discussed and studied is the time dilation of weak bursts relative to strong bursts. The attention to the time dilation effects due to its possible cosmological interpretation (Paczynski 1992). The results of time dilation measurements are different for different groups: Norris et al. (1994), Fenimore & Bloom (1995), Stern (1996) did find time dilation while Mitrofanov et al. (1996) and Lee & Petrosian (1997) claimed the absence of the time dilation.

¹Institute for Nuclear Research, Russian Academy of Sciences Moscow 117312, Russia, stern@al20.inr.troitsk.ru

²Stockholm Observatory, S-133 36 Saltsjöbaden, Sweden, {stern,juri,svensson}@astro.su.se

³Uppsala Observatory, Box 515, S-75120 Uppsala, Sweden

Positive detections of the time dilation were consistent with the simplest assumption that weak events are just redshifted (and therefore stretched) analogs of strong events. However in the work of Stern, Poutanen & Svensson (1997, hereafter SPS97), it was demonstrated that the situation is more complicated. Weak events are not only dilated (the general time dilation effect was confirmed), but they are also more asymmetric on average and have a different shape of slopes of the average time profile (ATP) which can be quantified in terms of different stretched exponential index.

Such brightness dependent correlations can easily be interpreted in terms of correlations between time properties and *intrinsic brightness*. Indeed, GRBs are composed of individual asymmetric pulses with fast rise and slower exponential decay (FREDs). A simple GRB consisting of one pulse is on average more asymmetric than a complex one where a chaotic bunch of overlapping pulses can produce an arbitrary time profile. A similar argument can be applied to the shape of the slopes of the ATP. If pulses have locally independent sources of energy, then complex events where the amplitudes of individual pulses sum up are intrinsically brighter than simple events. The direct morphological test performed by SPS97 confirmed this interpretation: complex bursts appeared systematically brighter than simple GRBs.

Although such correlations are natural in intrinsic brightness, we however observe them as a function of *apparent* brightness. This means that the distribution of GRBs over luminosity distance significantly differs from a power law (in the case of a power law, intrinsically strong and intrinsically weak GRBs would be blended in the same proportion at any apparent brightness). Of course, in a cosmological scenario, the distribution over luminosity distance differs from a power law even for a non-evolving rate of GRB production. However, the variation of the slope of the $\log N - \log P$ curve is too smooth (see, e.g., Mészáros & Mészáros 1996) to obtain such strong correlations in a narrow range of the apparent brightness (within one decade). This led SPS97 to the qualitative conclusion that a strong evolutionary factor is probably involved.

This work follows SPS97 in its main objectives. The larger statistics of GRBs is used, and, most importantly, the procedure of discriminating between simple and complex bursts is formalized and improved to a higher discrimination power. Due to the latter improvement, the direct test for a complexity - brightness correlation gave a very significant and meaningful result, which is described in § 3. Then, in § 4, we describe the results of our studies of the ATP shape as a function of brightness – these studies show further effects which are also associated with the complexity - brightness correlation. In § 5, we present a model example demonstrating how the above correlations can appear under simple assumptions and discuss the issue of the GRB intrinsic luminosity function. In the Appendix, we present a detailed description of the data analysis for the ATP study as well as a number of additional tests for possible systematic errors.

2. Data Analysis

This work is based on the data in the publically available Compton Gamma-Ray Observatory data archive at Goddard Space Flight Center. Our sample includes bursts up to trigger number 6230 and contains 1395 events selected as useful for complexity – brightness analysis and 1310 useful events for ATP study. We use 0.064 s and 1.024 s time resolution data from the Large Area Detectors (LAD). All the profiles are constructed in 64 ms resolution with an 1024 ms resolution extension if necessary and all background fits are done with 1024 ms data as they cover a wider time range including the pre-trigger history. We use the count rate summed over the four LAD energy channels, covering the 25 – 1000 keV energy range, when studying the behavior of the ATP, as well as channels 2–3 (50 – 300 keV) in complexity – brightness analysis. Backgrounds were subtracted using linear fits. A visual scan of all triggered bursts was performed in order to select useful events and to set fitting windows.

As a measure of the peak brightness of the event when sorting bursts into brightness groups we used the peak fluxes from the current BATSE catalog (Meegan et al. 1997) in 64 ms time resolution. Peak alignment and peak normalization of bursts were performed using count rates in 64 ms time resolution. In § 3 we use our estimations of the 64 ms peak count rate as a measure of brightness instead of peak fluxes from the catalog. In order to reduce brightness dependent biases associated with Poisson noise we developed a peak search scheme where each count rate excess over neighboring time intervals is tested for its statistical significance.

The important procedures of the data analysis and their tests are described in Appendix A.

3. Different Brightness Distributions for Simple and Complex Bursts

It is comparatively easy to distinguish between complex and simple events for the bright GRBs. One can then introduce a numerical measure of complexity, e.g., the total length of up and down variations normalized to the peak count rate. Alternatively, one can count runs up and down and use their number to characterize complexity (Lestrade 1994). Unfortunately, such an approach fails when dealing with weak GRBs because of the Poisson noise which heavily dominates any of the measures mentioned above (various attempts to filter out the noise do not help).

The only possibility to extract a “simple” subpopulation from weak bursts is to use the “canonical” shape of a single pulse, which are more or less identifiable by the human eye or by a χ^2 fit. The former approach was used by SPS97 in the form of a blind visual test. All events were rescaled to the same (low) brightness adding proper Poisson noise, then each rescaled event was classified by three test persons as “simple” (a single FRED pulse), or as “complex” (not a FRED pulse), or “unresolved” (usually too short to be confidently identified). Then peak brightness distributions for simple and complex GRBs were compared. Two of three test persons showed that complex GRBs are systematically brighter at a significance level exceeding 0.99, the third test person showed the same effect as a significance level 0.9. Now we present results using χ^2 tests for a larger statistics of GRBs.

3.1. The χ^2 Separation Between Simple and Complex Bursts

Unlike the visual test of SPS97, the χ^2 test is aimed at extracting events *dominated* by a single FRED pulse rather than consisting of a single FRED pulse. That is, the main peak was checked for how well it is fitted by the FRED’s pulse shape, while other smaller peaks not affecting the fit were allowed for an event to be qualified as “simple”. Pulses were fitted with the parametrisation of Norris et al. (1996): $I_{r,d}(t) = I_p \exp(-[|t - t_{\max}|/t_{r,d}]^\nu)$, where ν was allowed to vary between 0.9 and 2.2, t_{\max} to vary within ± 3 seconds around a direct estimate of the peak position, I_p , t_r , and t_d were free. The fitting interval was $(t_{\max} - 6t_r^{1/\nu}, t_{\max} + 6t_d^{1/\nu})$. The fit for each event was performed for 64, 128, 256, and 512 ms bins. The maximum value of χ^2 per degree of freedom (χ_m^2) for these four variants of binning was used for the classification. All events with a peak count rate > 55 counts/64 ms were tested (dimmer events were discarded), and all of them were rescaled to a peak count rate 55 counts/64 ms. All events with $t_r + t_d < 2$ s were discarded as the time resolution for short peaks at this brightness is insufficient.

A visual examination of the fitting procedure showed that it is not perfect, but this is natural. Sometimes a bright GRB which looks as an apparently complex dense bunch of pulses gave a good χ^2 when rescaled to low brightness, and sometimes a GRB looking like a FRED had a bad χ^2 not satisfying the parametrization (in such cases no human intervention occurred, of course). Nevertheless, in 90% of the events the result of the χ^2 test coincided with the visual impression, so we conclude that the above parametrization and the whole procedure work satisfactorily. Typically, the largest reduced χ^2 was obtained for the widest binning, 512 ms, this is also natural.

The number of resolved events for which the classification simple-complex was possible is 864 (of 1395 useful events). The distribution of χ_m^2 for these events is presented in Figure 1a. Note the striking difference in distributions for “fast risers” and “slow risers” which confirms that the test finds many really simple events among fast risers (which can be simple bursts) and almost none of them among slow risers (which should be complex bursts).

We found an apparent positive correlation between χ^2 and peak count rate (the reason why we use the peak count rate instead of the peak flux as the measure for brightness is discussed below). We separated bursts by different thresholds C_t in χ_m^2 and compared peak count rate distributions for simple ($\chi_m^2 < C_t$) and complex ($\chi_m^2 > C_t$) events estimating their consistency levels with a Kolmogorov-Smirnov (KS) test. The results are presented in Figure 1b. We see that without applying the $t_d > t_r$ criterion we have significance level for the brightness-complexity correlation $\sim 3 \times 10^{-4}$ (i.e, a disproof of the null hypothesis that the brightness distributions for simple and complex bursts are the same), while applying the $t_d > t_r$ criterion the significance level is $< 10^{-6}$ (minimum consistency level for identical parent distributions of simple and complex GRBs is 1.4×10^{-7}). Our final choice for the classification of a burst as “simple” is: $t_d > t_r$, $\chi_m^2 < 1.45$ (all other events satisfying $t_r + t_d < 2$ s are classified as complex).

3.2. Log N – Log P Distributions for Simple and Complex GRBs

We construct differential $\log N - \log P$ distributions for simple and complex events separately. These distributions corrected for the trigger efficiency (each class has its own efficiency) are presented in Figure 2. We plotted the number of bursts as a function of peak count rate, while the values for the peak flux from the current BATSE catalog (Meegan et al. 1997) corrected for the spacecraft orientation, number of triggered detectors, and reflection from the atmosphere could be a better measure of brightness. The effect in BATSE catalog peak flux distributions of simple and complex GRBs is similar: KS test gives a consistency level of 10^{-5} when using 1024 ms peak fluxes and 10^{-7} for 64 ms peak fluxes. Unfortunately, it is much more difficult to estimate the trigger efficiency as a function of the peak flux. The trigger efficiency is a much sharper and better defined function of the peak count rate than of the peak flux. This simplifies the problem of correcting for trigger efficiency when using peak count rate units.

The difference in the behavior of the $\log N - \log P$ distributions for the two classes of GRBs is striking. While the curve for simple events is consistent with a power law down to the trigger threshold, the complex class demonstrates an apparent break at a brightness exceeding the threshold by a factor of 3 – 5. If one shifts the “complex” distribution by a factor $1/k < 1$ discarding bursts moving below threshold (i.e. $P/k < 55$ counts/64 ms) then the KS consistency level peaks at $k = 2.1$ which can be interpreted as complex events being ~ 2 times brighter on average. This factor can be even larger, this depends on the behavior of the “simple” distribution below threshold.

The main difference in the brightness distributions is concentrated at the low brightness range and can be described as a relative deficit of complex bursts by factor ~ 2 near threshold. The low brightness range may contain systematic biases (threshold effects) and we must estimate them before drawing any conclusions. We have no reason to suspect the rescaling procedure as being a source of bias as this procedure is trivial and one can exactly account for the variation of noise when we rescale burst to the same brightness. Another possible bias can be associated with the errors of the background fits, but this bias is of the opposite sign of the effect: weak bursts should give a higher χ^2 due to nonzero residuals outside of the peak. The visual classification of SPS97, which is less sensitive to rescaling and insensitive to the background subtraction gave a similar result.

We also cannot suspect systematic errors in the estimates of the peak count rates. The reasonable linearity of this estimate is demonstrated in Appendix A (Fig. 8). A correlation between complexity and the peak count rate estimates could exist but it is a 10% effect, while a factor 2 bias is required to account for the effect. A more serious source of systematic error could be a different trigger efficiency for simple and complex events. Indeed, slow risers, which have lower trigger efficiency, mostly belong to the complex sample. In order to verify this, we calculated the trigger efficiency separately for simple and complex events as described in Appendix A (the distributions in Fig. 2 as well as the significance levels given above are already corrected for different trigger efficiencies).

The efficiency for complex events is actually lower, e.g, at the peak count rate 55 counts/64 ms it is 0.69 for simple events and 0.56 for complex bursts. Nevertheless, the difference is negligible comparing to that required to explain the effect: at least a correction by a factor 2 applied only to complex weak bursts is required to make the distributions consistent. We can hardly admit as explanation that it is a result of a huge unknown selective bias which affects only high χ^2 bursts but does not affect low χ^2 events. Indeed, we suggest that the upper curve in Figure 2, representing presumably intrinsically strong events, extends to larger cosmological distances, where some effect associated with high redshifts becomes important. Then, it is natural to suggest that the lower curve will show a similar behavior below the threshold.

Can the distribution of the complex bursts be fitted with a nonevolving cosmological model? The break seems too sharp to allow such a fit. It is much more natural to suggest that the intrinsically strong subpopulation of BATSE GRBs extends to $1 < z < 2$ where the Universe evolves strongly. The evolution at this age is clearly visible in the QSO redshift distribution (Hartwick & Schade 1990) and in the star formation rate curve (Madau et al. 1996; Abraham 1997) In the neutron stars merging scenario (Blinnikov et al. 1984; Paczyński 1992) the GRBs rate should be associated with the star formation rate (Lipunov et al. 1995; Prokhorov, Lipunov, & Postnov 1997). In this case, the break in the $\log N - \log P$ curve for complex GRBs should correspond to the peak in the star formation rate at $z \sim 1.5$.

4. Brightness Dependent Correlations in the Average Time Profile

After confidently observing complexity - brightness correlations, the ATP - brightness correlations can be considered as a direct consequence of the former. Nevertheless, they still provide an independent confirmation for the correlation tendency, complete the picture, and are interesting in themselves. For this reason, we present the latest results of the ATP studies with a more detailed description than was given in SPS97.

4.1. On the Stretched Exponential Shape of the ATP

The claim of the stretched exponential (SE) shape of ATP, $F(t) = F_0 \exp[-|t/t_0|^\nu]$, has been done by Stern (1996) for the decaying slope and confirmed with successively higher statistics by Stern & Svensson (1996) and SPS97 (in the latter work the SE shape of the rising slope of ATP was demonstrated). Both rising and decaying slopes of ATP for the overall useful BATSE statistics (1310 events) are presented in Fig. 3a. The high statistics demonstrates that picture is more complicated than the idealized assumption accepted in SPS97: i.e rising and decaying parts have not only different time constants but also different shape (SE index, ν): the decaying ATP is perfectly described by a SE with $\nu = 0.37$, while the rising ATP is described by a SE with $\nu = 0.30$. Note that the whole “disorder” comes from weakest bursts. If we remove them, both the rising and decaying ATPs are much closer to the “canonical” shape with $\nu = 1/3$ (Fig. 3a). The

different ATP shape of the weakest bursts was noted by SPS97. The difference is significant and cannot result from the trigger selection effect. The interpretation of this fact is discussed below, for now we just note that:

- SE with $\nu = 1/3$ for both slopes is still good working hypothesis for stronger bursts.
- For the full sample, SE indices of rising and decaying ATPs differ, the difference is real and significant. However both ATPs are still described by SEs. We demonstrate below that the difference in ATP shapes is a natural consequence of asymmetric shape of elementary pulses.

Let us now consider an issue whether the stretched exponential shape of ATP is just a successful fitting hypothesis among other comparable possibilities or it is a natural intrinsic feature of ATP?

Log F - Log t plot of ATP demonstrates that it does not resemble power law in any range of time. Nevertheless, Mitrofanov, Litvak & Ushakov (1997) used the fitting expression with power law asymptotics, $F(t) = [t_0/(t_0 + t)]^\alpha$, to fit the ATP (here constants t_0 and α are different for two slopes). Introducing the third parameter, general multiplier β , we are getting the best fit for the decaying part of ATP in 0.125 - 216 seconds range with $\chi^2 = 128$ for 19 degrees of freedom (Fig. 3b) and unreasonably small value at $t = 0$: $\beta = 0.62$. Since Mitrofanov et al. (1997) constructed ATP in 1024 ms resolution (i.e. the $t < 1$ s fragment was lost) and only within $t < 20$ s range, it is not surprising that they obtained a good fit in this narrow interval. However, for a wider interval this parametrisation is unacceptable.

Let us take as another example a log-normal distribution which is quite common in Nature. It has wrong asymptotics at $t = 0$, but we ignore this by setting $F(t) = \beta \exp(-\log^2(t/t_0)/2\sigma^2)$ at $t > t_0$ and $F(t) = \beta$ at $t < t_0$. This semi-artificial expression fits ATP in the same range as above with $\chi^2 = 89$ for 19 degrees of freedom and again with unsatisfactory value at $t = 0$: $\beta = 0.6$ (see Fig. 3b). For comparison, a stretched exponential fit of the same profile gives $\chi^2 = 4.1$ at $\nu = 0.37$, $t_0 = 1.12$ and $\beta = 1.04$. For a reasonability of the χ^2 values see Appendix B.

We can make a bet that no one 3-parametric expression will fit the ATP except the SE. Note, that our SE fit is in fact “2.5-parametric”, i.e. the third parameter, multiplier β , just accounts for an uncertainty associated with first 64 ms bin of ATP, assumed to be close to 1 and its best fit value is actually always close to 1.

Summarizing the issue, we state that the stretched exponentiality of the ATP is probably not exact. However, with the existing statistics we do not see any statistically significant deviations. The SE is a natural distribution shape involving a wide range of time scales occurring in very different classes of phenomena (Ching 1991; Jensen, Paladin, & Vulpiani 1992). Therefore we believe that our choice of SE as the fitting expression is not only efficient but also meaningful.

The procedures of measurement of SE time constants of ATP and estimates of statistical errors follow SPS97. They are described in more details in Appendix B.

4.2. Time Constants of the ATP as a Function of Brightness

In our studies of the ATP behavior, we used two kinds of SE fits. The first is the simultaneous fit of both ATP slopes with SEs of the same index, $\nu = 1/3$, and common normalization factor β . This 3-parametric fit (t_r , t_d , and β) has the best statistical accuracy. The results of these SE fits are summarized in Table 1 and in Figure 4.

In comparison to the GRBs statistics used by SPS97 (912 events) the time dilation of the decaying slope is slightly larger, $t_{d,9}/t_{d,7} = 1.89^{+0.68}_{-0.44}$ (90% confidence interval) comparing samples 9 and 7 (see Table 1). The time dilation is now more significant. The corresponding rejection level for a null hypothesis (no time dilation) increased up to 0.99995 (assuming a normal for distribution of the deviations of the values). The time dilation of the rising slope also slightly increased, but still remains at a low significance level. The resulting variation of the asymmetry (the ratio t_d/t_r) slightly decreased. Comparing samples 1 and 9 we get: $(t_d/t_r)_{\text{dim}}/(t_d/t_r)_{\text{bright}} = 1.48^{+0.55}_{-0.32}$ (90% confidence interval). The significance level for this correlation remains the same as for the SPS97 sample, ~ 0.02 . The general time dilation of $t_r + t_d$ has a statistical significance 4×10^{-4} ; the “dim/bright” ratio is $(t_r + t_d)_9/(t_r + t_d)_7 = 1.71^{+0.62}_{-0.38}$ (sample 9 compared with sample 7).

The results presented so far were obtained with a fixed SE index, $\nu = 1/3$. Now we present a second fitting variant. As was mentioned above, the ATP for the whole sample indicates a larger ν for the decaying slope and a lower ν for the rising slope. Despite the fact that the difference results from the contribution of weak GRBs, it would be interesting to check the behavior of time constants when ν is fixed to different values for the two slopes. Unfortunately, we cannot then use a common β for both slopes, this would lead to unacceptable values of χ^2 . Therefore, we performed *independent* 2-parametric fits ($\beta, t_{r,d}$) for both slopes which gives a 20% worse accuracy, setting $\nu_r = 0.30$, $\nu_d = 0.37$. With such a fit, t_r becomes systematically smaller (by factor 0.51), and t_d systematically larger (by factor 1.6). Such an effect on the time constants is due to the strong correlation $\nu - t_{r,d}$ (see Fig. 10 in Appendix B). These time constants rescaled by a factor $1/0.51$ and $1/1.6$ are shown in Figure 4. One sees that the behaviors of these time constants with peak brightness are the same. The variation of the asymmetry is even slightly larger than for the first fitting variant.

A test for the presence of brightness dependent biases in these results is described in Appendix A. Only the weakest sample 6 is affected by trigger selection bias and by Poisson noise. For this reason, sample 6 was excluded from the analysis of the brightness dependent correlations. To test for spectral redshift of weak bursts as being the possible explanation of the asymmetry variation, we measured the asymmetry in separate LAD’s energy channels. If GRBs were more asymmetric at higher energies, then the spectral redshift of the softer, more symmetric, component to energies below the observation band could cause an asymmetry – brightness correlation. The results are presented in Table 2. One sees no tendency supporting such a hypothesis: GRBs have the same asymmetry in all channels.

4.3. Variations of the Stretched Exponential Index with Brightness

Figure 5 presents the decaying and rising slopes for samples 1+2, 3+4 and 5+6. Except for the apparent time dilation effect, the deformation of the weakest ATP is clearly visible. Partially, this deformation results from brightness dependent bias (short weak bursts have smaller trigger efficiency and the peak searching scheme is unable to find the sharp peaks of longer events, also see Fig. 9). This bias suppress the ATP within 1 s from the peak while its effect beyond 1 s is not so strong.

The estimate of the significance level for the shape variation is difficult because trigger selection and Poisson biases give deformations of the same sign (but still much smaller) as observed. SPS97 estimated the significance level of deformation of the decaying slope for the weakest sample as 0.95 after correcting for the above biases and possible error of the background subtraction. We do not make this estimate here, because the deformations of the ATP must appear as the direct consequence of the much more significant complexity – brightness correlation described above.

5. On the Issue of the Intrinsic Luminosity Function

We used, as most researchers do, the burst’s peak amplitude as a zeroth order approximation measure of the luminosity distance (a standard candle) — this was assumed when we selected brightness groups using this parameter. The fact that we see correlations between the shape of the average profile and brightness tells us that the peak amplitude is a bad standard candle, and that the intrinsic peak luminosity function is a broad distribution where the average time profile of events depends on the peak luminosity. What could serve as a better standard candle?

Some researchers suggest that the total energy fluence is a better standard candle than the peak luminosity (e.g. Petrosian & Lee 1996) arguing that this would be more physical. However, this approach has at least two serious problems:

- A huge range of luminosity distance (short weak bursts have about 4 orders of magnitude smaller apparent fluence than long strong bursts). Then one can expect either large relative redshifts or Euclidean scaling for long bursts. Neither of these is observed.
- A strange “time shrinking” for more distant GRBs (see Lee & Petrosian 1997).

If we accept that something like the pulse avalanches of Stern & Svensson (1996) takes place, then a dispersion in the fluence of a few orders of magnitude seems natural. The GRB itself emits just a fluctuating fraction of the total energy release, and probably there are many events where an observer sees no GRB. The pulse avalanche model describes the transmission of energy from a main reservoir as a highly unstable near-critical process, where in the idealized case of exact criticality and infinite available energy, the fluence distribution should become a power law.

A better candidate for the standard candle would be a single pulse independently of whether

it alone constitutes a burst or appears as one of the pulses in a complex bursts. Again the peak amplitude of a pulse seems more constant than its fluence (for studies of fluence distribution of pulses in GRBs, see Li & Fenimore 1996) – otherwise a negative correlation between pulse duration and its amplitude within one GRB would be visible. Does any correlation exist within one event? The visual impression from GRBs light curves is that there is no evident correlation. Unfortunately such a correlation is not easy to extract as pulses tend to overlap and it is very easy to take a dense bunch of narrow pulses for a single pulse. From our unpublished pulse avalanche simulations it seems that the duration - amplitude correlation for pulses should be weak and rather positive than negative.

Actually amplitudes should be distributed somehow. Let us consider, as an example, the log-normal distribution for the pulse peak amplitude (the same was found by Li & Fenimore 1996 for pulse fluences). Using this distribution in the pulse avalanche simulations we then the corresponding intrinsic luminosity function for simulated bursts caused by piling up of pulses. We then apply to our simulated bursts the same procedure of χ^2 selection that was used to separate simple and complex real GRBs. The difference in the distributions of intrinsic luminosities of simple and complex events in this example (see Fig. 6) seems sufficient to cause a difference in the behavior of their $\log N - \log P$ curves in the presence of a strong evolutionary effect (the ratio of medians of the distributions is 3.7).

The recent work of Pendleton et al. (1997) found similar effect that separating GRBs into subclasses affected the $\log N - \log P$ distribution. They use a very different parameter from us: the presence of a hard tail in the spectrum, i.e., significant emission above 300 keV. We suggest that the “non high energy” and “high energy” subclasses of Pendleton et al. (1997) probably correlate with our simple and complex groups, respectively.

6. Summary and Conclusions

The effects we confidently detect can be summarized as follows:

1. Complex bursts are systematically brighter than dim bursts. Their brightness distribution has an apparent break at a count rate ~ 200 counts/64 ms which exceeds the threshold by a factor four.
2. Weaker bursts have a stronger asymmetry between the rising and decaying slopes of the average time profile.
3. The weakest bursts have a different shape of their slopes of the average time profile, which can be described as a larger stretched exponential index (at least for the decaying slope).
4. The general time dilation of weak bursts is complicated by the deformations of the ATP resulting from the two previous effects.

Effects 2) and 3) appear as direct consequences of effect 1). The effect 4) can result both from

cosmological time dilation (Paczynski 1992) and from intrinsic brightness - duration correlation (Brainerd 1994). Effects 1) – 3) can appear as a result of the correlation between temporal properties of GRBs and their intrinsic brightness only if we discard as explanation an evolution of GRBs temporal properties with time which seems unnatural. The large value of these effects indicates that the intrinsic luminosity function is a wide one: comparable with the brightness dispersion from the distance distribution. Therefore the $\log N - \log P$ curve can be a convolution of two functions of comparable dispersions. The work of Pendleton et al. (1997), where they demonstrate how a selection of GRBs based on their spectral properties affects $\log N - \log P$ curve, supports this conclusion.

Both the most confident and the most informative effect is the first one. There is no obvious source for such a high near-threshold bias (selective for simple and complex events) to account for this effect. There is, however, a natural phenomenon that could account for it. As was already mentioned above, this could be the evolution of the star production rate. We must accept this as a possible explanation if we accept the merging of neutron star binaries as the source of GRBs.

It seems that we succeeded to extract an intrinsically strong subsample from the BATSE GRBs which covers distances to $z \sim 1.5$ distances where evolutionary effects should be strong. A cosmological fit with an evolutionary factor for GRBs based on the measured star formation rate and with model luminosity function similar to that presented in § 5 is a matter for separate work. The crucial data to confirm this point of view could appear from the search for untriggered bursts in the continuous BATSE data records. This search is ongoing (Kommers et al. 1997) and is worth intensifying.

We thank Felix Ryde for helpful assistance. This study made use of the data provided by the Compton Observatory Science Support Center. We are grateful to the BATSE team for a fast supply of the new data to the publically available database. This research was supported by grants from the Swedish Natural Science Research Council, Stockholm University, the Swedish Royal Academy of Sciences, and a NORDITA Nordic Project grant.

A. Data Analysis

A.1. Background Fitting

The background fitting was based on a visual scan of all BATSE bursts. This work cannot be done automatically because there exist many events with complex backgrounds contaminated with non-Poisson features which can mimic the contribution of a GRB. In fact, each individual burst requires a researcher’s decision – how to fit it or whether it should be discarded. To avoid subjective biases for weak events, we followed the rules described below:

1. All fits are linear (the background anyway often demonstrates a non-polynomial behavior and a higher order polynomial fit could be unstable). Linear fits were made over one or two “fitting

windows”, which were set in “quiet” intervals, having a good χ^2 . We also set the “observational” windows avoiding background features not associated with the burst. In the case of a smooth curved background with several burst episodes in the event, we set a few fitting windows including quiet intervals between burst episodes, so the background was approximated by a broken line.

2. Each feature separated by a wide time interval from the main peak should be tested whether it came from the same direction as the main peak. To compare directions we made a linear fit to the count rate in the interval covering the feature for each of eight LADs. We then maximized the total reduced χ^2 in the interval varying time resolution, and calculated the eight-component vector χ^2 . This vector should approximately be parallel to that of the main peak, otherwise the feature should be avoided when setting observational windows. The procedure turned out to be an efficient way to clean up bursts from unrelated fluctuations.

3. We adopted a default set of windows: a fitting window ($-120\text{ s} - -70\text{ s}$, where the boundaries are given respectively to the trigger time), an observational window ($-70\text{ s} - +200\text{ s}$), and a second fitting window ($+200\text{ s} - +250\text{ s}$). If possible, we used the default set. If the background has a moderate curvature – it should not give a bias as it has a random sign. This rule reduces a possible subjective bias. A narrower interval between fitting windows was allowed if the burst was apparently short or the background was strongly curved.

4. All events where we were unable to make a confident conclusion that we did not loose and did not contaminate the signal at 100s after and 50s before the highest peak, were discarded. This could be due to wide data gaps, strong solar flares, rapid variations of the background, or chaotic variations with bad χ^2 from the wrong direction.

This fitting procedure gives as small bias as possible when summing up signals from different GRBs to get the average time profile, despite the fact that it is not accurate when dealing with individual events. To estimate the magnitude of possible errors introduced by the fitting procedure we made the following test. For each event where it was possible ($\sim 75\%$ of all events), we selected testing windows between our fitting windows avoiding regions with GRBs signals and measured the residuals to our fits in the testing windows. The distribution of residuals for 469 weak and medium events is shown in Figure 7. The distribution of residuals is reasonably symmetric, the average value for the residual is $+0.084$ counts/64 ms, the 1σ variance is 1.43 counts/64 ms. This is an argument that we have no significant systematic error (that exceeds the statistical error). The statistical error for the average residual is 0.11counts/64 ms. For comparison, the typical background in channels 2 and 3 is 300 counts/64 ms, the peak count rate for weakest events is ~ 50 counts/64 ms. The error introduced into the average time profile is inversely proportional to the peak count rate. For medium and bright events we can neglect the fitting uncertainty – it is much less than 10^{-3} . The exception is the weakest group where the 1σ error in the relative averaged residual is 1.5×10^{-3} .

A.2. Selection of the Highest Peak

The direct peak selection using the highest 64 ms bin, while working good for bright events, suffers from Poisson noise for weak events. It just takes the highest Poisson fluctuation as being the burst’s highest peak. Nevertheless, as far as we adopted the 64 ms resolution approach, we should not use a different time resolution for weak bursts. As a compromise, we developed a hybrid scheme which combines a search for the peak interval in a lower time resolution and a search for statistical significant deviations in this interval with a higher time resolution.

First, we determine the shortest time-scale $\Delta t_j = 64 \text{ ms} \times 2^j$, $j = 0, \dots, 4$, where a GRB has statistically significant variations between neighboring time bins (a 7σ threshold, which corresponds to a 5σ threshold for a deviation from the average). Then we search for the highest peak centered at bin number k using the time resolution, Δt_j , and calculating the peak flux as $\max\{\sum_i c(i) \exp[-((k-i)/2^j)^2]\}$ where k and i are indices of 64 ms bins, and $c(i)$ is the count rate in the i -th bin.

Then, if $j \geq 1$ we make a second iteration: searching for statistically significant excess over average within the brightest Δt_j interval using a shorter time-scales. The significance threshold, h_l ($l < j$), is reduced at this step. The thresholds were optimized empirically when tuning the scheme by rescaling strong bursts to the weakest, adding corresponding Poisson noise, selecting the highest peak, and comparing resulting peak amplitude and position with true values. With thresholds $h_0 = 4.0\sigma$, $h_1 = 3.2\sigma$, $h_2 = 2.0\sigma$, and $h_3 = 1.2\sigma$ above the average count rate in Δt_j we obtain a reasonable linearity between the expected and the measured count rate and still preserve the 64 ms resolution.

A test of this procedure by rescaling strong events to a given value of peak count rate is presented in Figure 8. The rescaling procedure is described in § A.3. Only those events which passed our simulated trigger after rescaling were included into the test distributions. One can see from Fig. 8a. that we have a reasonable linearity between the measured and the expected peak count rates (compare with a similar plot in Fig. 2 of in ’t Zand & Fenimore 1994). The systematic bias in the peak amplitude for the weakest events is within 3%, the relative error is $\sim 35\%$ (FWHM) for $P=55$ counts/64 ms and $\sim 22\%$ for $P=110$ counts/64 ms. There are non-Gaussian tails towards higher values associated with Poisson fluctuations however they do not exceed a few per cent of the peak integral. If one increases the thresholds, these tails will disappear, but a nonlinear bias of peaks towards lower values will appear. The thresholds have been set as a compromise where we have a reasonable average linearity of peak count rate estimates for weak events. (Note that direct selection of the highest bin in 64 ms resolution systematically overestimates the peak amplitude by a factor of 2 for the weakest events). The errors in the peak position can be characterized as follows: in 35% of the cases, the error does not exceed one 64 ms bin, with 47% probability the error is within 0.128 s, with 83% probability it is within 1 s, and in 6% of the cases the error exceeds 3 s.

A.3. The Estimation of the Trigger Efficiency

We estimated the trigger efficiency assuming that GRBs of near-threshold brightness do not differ in their temporal properties from stronger GRBs (which is not exactly true). The procedure consists of the following steps:

1. For a given peak count rate P_0 , sample randomly one of the stronger bursts with a peak count rate $P > P_0$ of the same class (i.e., simple or complex) for which we are going to estimate the trigger efficiency and subtract the background thus extracting a pure signal.
2. Sample randomly another strong event of arbitrary class in order to use its linear background fit.
3. Rescale the signal by factor P_0/P and distribute it between the two detectors having the largest projected areas for a randomly sampled direction of the burst. Distribute the signal proportionally to their projected areas. This step does not take into account the reflection from atmosphere which causes more uniform exposure of the detectors thus enhancing the trigger efficiency. The procedure also ignores the dependence of the detector response matrix on the projection angle. This dependence also enhance the trigger efficiency. Thus, our procedure slightly underestimates the trigger efficiency. It also neglects the probability of triggering three detectors for weak bursts.
4. Add a new linear background from two arbitrary detectors of the event sampled at step 2 and a corresponding Poisson noise (taking into account that some noise is already there in the rescaled signal).
5. Try the trigger procedure to the rescaled burst as it is programmed in BATSE (with the 5.5σ threshold that was used most of the observation time, see Meegan et al. 1997).

The fraction of rescaled bursts triggered with this procedure is the trigger efficiency. Note that with such a procedure the trigger efficiency is a function of the *expected* count rate.

A.4. Robustness of the ATP: Test for Brightness Dependent Biases

Brightness dependent errors in the ATP induced by Poisson noise are:

- Errors in the peak count rate estimate which is used as the normalization of a time profile,
- Errors in the peak position,
- Trigger selection effects which removes short or short spike dominated events from the sample.

We estimated the brightness dependent deformations of the ATP by rescaling strong events to low peak count rates and applying simulated trigger selection to the rescaled sample. The parent sample included 353 GRBs with the highest peak count rates of all morphologies and durations.

The results are presented in Table 4 and in Figure 9.

We can state that down to the sample 5 of Table 1 deformations of the ATP are negligible (the count rate 110 counts/64 ms is near the boundary between samples 5 and 6) and only for sample 6 (75 counts/64 ms) are they significant. Therefore we can measure the variation of the ATP slopes without the rescaling procedure which would have erased some information for strong samples.

B. Stretched Exponential Fits and Their Errors

As was noted in Stern (1996), the main problem when fitting ATPs is the correlation of deviations in different time bins (the profile is the sum of more or less smooth but very different curves). This means that one cannot rely on deviations of individual profiles in a χ^2 fit, especially when estimating the accuracy of this fit. In principle, a proper solution of the problem should exist and it should require an overall correlation matrix implemented into the maximum likelihood method, but we expect that such a solution is not an easy one. In Stern (1996), the errors were estimated using a number of smaller samples of bursts. The variance of the time constants derived from the smaller samples was then rescaled to larger samples as $1/\sqrt{N}$, where N is the number of bursts in a sample. With a limited statistics such a procedure can only give a very approximate estimate of the errors and is very unreliable if one uses it to estimate the statistical significance level of observed effects.

Following SPS97 we estimate the statistical errors using the pulse avalanche model simulations. Here we present further details of the procedure. For a description of the pulse avalanche model, see Stern & Svensson (1996). The general time-scale in the model is defined mainly by an upper cutoff for the pulse width distribution. It was tuned to get desirable time constants for the stretched exponential average time profiles. Another parameter that was varied is the “criticality index”, μ , which defines the Poisson average of baby pulses per parent pulse in the avalanche. At supercritical values of μ , the process diverges. Varying this index some finer features like the stretched exponential index and the rise/decay asymmetry of the average time profile could be tuned. We, however, varied μ mainly in order to test a possible model-dependency of the statistical errors.

We found that the rise/decay asymmetry of the ATP can be described better when we introduced a “global envelope”, to be more exact, an external time dependence for the criticality index, $\mu = \mu^0 \exp(-t/T)$, where the “global” time constant T is large ($T = 400 - 600$ s). Then the main peak tends to appear earlier, the rise/decay asymmetry is therefore enhanced. Such a global envelope with a large time constant seems natural in many scenarios of GRB emission. T is one of the variable parameters in the present study ranging from 200 s to infinity.

To fit the ATP one needs to split the ATP into a number of bins. This number should not be too large, otherwise neighboring bins will be too strongly correlated and the value of χ^2 or of other likelihood estimators would be completely meaningless. We choose equidistant binning

in the $t^{1/3}$ scale, each bin being $0.25\text{ s}^{1/3}$ wide. Correlations are still strong, but with a wider binning we could lose some information. Our value of χ^2 is still not usable as a direct estimator of the quality of the fit, but using the model we can calculate the distribution of χ^2 for many “intrinsically good” (i.e., giving a good stretched exponential at high statistic) ATPs and then define the actual effective number of degrees of freedom and the renormalization coefficient for χ^2 (see below).

When fitting an ATP for a sample of N bursts, we must know how the deviations in each time bin are distributed for many independent samples. We calculated such distributions using $N \times K$ simulation runs which produce K independent samples of N events each (typically $K = 500$ and N vary from 100 to 1000). We found that the deviations are excellently described by a “continuous Poisson” distribution, or, in other terms, by a gamma-distribution: $F(x, a) = a^x e^{-a} / \Gamma(x + 1)$, where x is the distributed value, and a is a parameter equivalent to the Poisson average (traditionally gamma-distribution is used with a being the distributed value and $x - a$ a parameter).

We found that the Poisson average a in bin j for all studied cases can be parameterized as $a_j = p_j N g(p_j) f(p_j N)$ where p_j is the ATP value in the bin (averaged over $N \times K$ events), g and f are slowly varying functions: g varies between 3 and 5, $f(x) = 1$ at $x > 2$ and smoothly decreases at $x < 2$. Then the standard maximum likelihood procedure was applied with an estimator $\chi^2 = -2 \sum_j \ln[F(p_j - h_j, a_j) / F(a_j, a_j)]$, where h_j is our hypothesis: $h_j = \beta \exp[-(t/t_0)^{1/3}]$. At large values of a_j , this expression coincides with the traditional χ^2 estimator.

We need two kind of fits depending on the aim. If we are interested in the shape of the ATP slope, we use a 3-parametric fit: $F(t) = \beta \exp[-(t/t_0)^\nu]$, where β , ν , and t_0 are free parameters with the additional requirement that β is close to 1 which is fulfilled in all reasonable cases.

With pulse avalanche simulation runs (500×400) and (500×1000) we found that the error in the best fit estimate for ν is: $\sigma_\nu / \nu = 0.049 \times \sqrt{1000/N}$ where N is the number of events in the sample. The cross-correlation of t_0 and ν for a pulse avalanche simulation run (200×750) is shown in Fig. 10. One can see that it is very strong and the error for t_0 is large for a free ν .

However, if we are interested in the behavior of time constants as a function of brightness we should fix ν . Indeed, we can compare time constants only with a hypothesis that the ATPs have the same shape (i.e., the same SE index ν) intrinsically. Our studies demonstrate that this hypothesis is not exactly true (see § 4). Nevertheless, the measurement of t_0 with constant ν is still the best that can be done. The deformation of the slope, if moderate, gives a second-order error. Therefore we measure t_0 with a 2-parametric fit.

In principle, one can set $\beta = 1$ and make a one parameter fit, but the first bin includes all possible biases from the finite resolution and the Poisson noise. We therefore excluded the first two bins ($t^{1/3} < 0.5$) from the fit treating β as a free parameter. The upper limit for the fitting range was set to $t^{1/3} = 5$ (i.e., $t = 125\text{ s}$).

As far as we have two slopes of the profile — pre-peak and post-peak, we fitted them

simultaneously with different time constant, t_r (pre-peak, rising slope), t_d (post-peak, decaying slope), and a common β . Performing a number of model runs with different parameters, we found the accuracy of the stretched exponential fits to be almost model-independent. The standard deviation for the time constant does not change more than by 5% for different parameters and scales as $1/\sqrt{N}$ depending on the number of events in the sample. The accuracy slowly increases, when the fitting time interval is extended (see Table 5). We chose the widest interval, which is the default for the results presented elsewhere in the paper.

For the sum and ratio of time constants for pre-peak and post-peak slopes we have:

$$\begin{aligned}\sigma(t_r + t_d)/(t_r + t_d) &= 0.196\sqrt{100/N}, \\ \sigma(t_d/t_r)/(t_d/t_r) &= 0.135\sqrt{100/N}.\end{aligned}\tag{B1}$$

Note, that the relative accuracy for the sum of time constants is close to that for one constant while the accuracy for their ratio is considerably better. This results from the strong correlation between the two slopes – a circumstance that favors the measurement of shape - brightness correlations and complicates the measurement of a time dilation effect.

As was mentioned above, the formal values of the χ^2 have no direct interpretation, the Pearson criterion does not work in this case because of strong correlations along the ATP. This could be interpreted as the effective (unknown) number of degrees of freedom being smaller than the numbers of bins. Actually the distribution of χ^2 becomes wider for a larger number of events in the sample. In Figure 11 we present two distributions of χ^2 for simulated samples which could be used for an approximate evaluation of the goodness of χ^2 obtained in the ATP fittings of real GRB samples.

REFERENCES

- Abraham, R. 1997, *Nature*, 387, 850
- Blinnikov, S. I., Novikov, I. D., Perevodchikova, T. V., Polnarev, A. G. 1984, *Sov. Astron. Lett.*, 10, 177
- Brainerd, J. J. 1994, *ApJ*, 428, L1
- Ching, E. 1991, *Phys. Rev. A*, 44, 3622
- Fenimore, E. E., & Bloom, J. S., 1995, *ApJ*, 453, 25
- Hartwick, F. D. A., & Schade, D. 1990, *ARA&A*, 28, 437
- in 't Zand, J. J. M., & Fenimore, E. E., 1994, in *Proc. 2nd Huntsville Gamma-Ray Burst Workshop* (New York: AIP), eds. G. J. Fishman, J. J. Brainerd, & Hurley K., p. 692
- Jensen, M. H., Paladin, G., & Vulpiani, A. 1992, *Phys. Rev. A*, 45, 7214
- Kommers, J. M., Lewin, W. H. G., Kouveliotou C., van Paradijs, J., Pendleton, G. N., Meegan, C. A., Fishman, G. J. 1997, *ApJ*, in press (astro-ph/9707171)
- Lee, T. T., & Petrosian, V. 1997, *ApJ*, 474, 37
- Lestrade, J. P. 1994, *ApJ*, 429, L5
- Li, H., & Fenimore, E. E. 1996, *ApJ*, 469, L115
- Lipunov, V. M., Postnov, K. A., Prokhorov, M. E., Panchenko, I. E., & Jorgensen, H. 1995, *ApJ*, 454, 593
- Madau, P., Ferguson, H. C., Dickinson, M. E., Giavalisco, M., Steidel, C. C., & Fruchter, A. 1996, *MNRAS*, 283, 1388
- Meegan, C. A., et al. 1997, *Current BATSE Gamma-Ray Burst Catalog*,
<http://www.batse.msfc.nasa.gov/data/grb/catalog>
- Mészáros, A., & Mészáros, P. 1996, *ApJ*, 466, 29
- Mitrofanov, I. G., Chernenko, A. M., Pozanenko, A. S., Briggs, M. S., Paciesas, W. S., Fishman, G. J., Meegan, C. A., & Sagdeev, R. Z. 1996, *ApJ*, 459, 570
- Mitrofanov, I. G., Litvak, M. L., & Ushakov D. A. 1997, *ApJ*, in press (astro-ph/9707128)
- Norris, J. P., Nemiroff, R. J., Scargle, J. D., Kouveliotou, C., Fishman, G. J., Meegan, C. A., Paciesas, W. S., & Bonnell, J. T. 1994, *ApJ*, 424, 540
- Norris, J. P., Nemiroff, R. J., Bonnell, J. T., Scargle, J. D., Kouveliotou, C., Paciesas, W. S., Meegan, C. A., & Fishman, G. J. 1996, *ApJ*, 459, 393

- Paczynski, B. 1992, *Nature*, 355, 521
- Pendleton, G. N., et al. 1997, *ApJ*, 489, in press
- Petrosian, V., & Lee, T. T. 1996, *ApJ*, 467, L29
- Prokhorov, M. E., Lipunov, V. M., & Postnov, K. A. 1997, in *Proc. XXXII Rencontres de Moriond, Les Arcs, France*, in press (astro-ph/9704039)
- Stern, B. E. 1996, *ApJ*, 464, L111
- Stern, B. E., & Svensson, R. 1996, *ApJ*, 469, L109
- Stern, B. E., Poutanen, J., & Svensson, R. 1997, *ApJ*, in press, astro-ph/9703167 (SPS97)

#	Peak flux	N	t_r	t_d	$t_r + t_d$	t_d/t_r	χ^2
1	12 – ∞	84	0.29 \pm 0.08	0.36 \pm 0.07	0.65 \pm 0.13	1.23 \pm 0.17	7.6
2	3 – 12	282	0.35 \pm 0.04	0.51 \pm 0.06	0.87 \pm 0.09	1.47 \pm 0.11	6.9
3	1.75 – 3	239	0.37 \pm 0.05	0.64 \pm 0.08	1.01 \pm 0.12	1.74 \pm 0.21	4.8
4	1 – 1.75	358	0.45 \pm 0.05	0.73 \pm 0.07	1.17 \pm 0.11	1.63 \pm 0.11	21
5	.7 – 1	196	0.43 \pm 0.06	0.74 \pm 0.10	1.17 \pm 0.15	1.70 \pm 0.15	22
6	0 – .7	151	0.38 \pm 0.06	0.77 \pm 0.11	1.15 \pm 0.17	2.00 \pm 0.20	29
7	7.5 – ∞	145	0.29 \pm 0.05	0.38 \pm 0.06	0.67 \pm 0.10	1.33 \pm 0.14	11
8	5 – ∞	209	0.29 \pm 0.04	0.41 \pm 0.05	0.71 \pm 0.09	1.40 \pm 0.12	9
9	.8 – 2.5	659	0.43 \pm 0.04	0.72 \pm 0.06	1.15 \pm 0.09	1.68 \pm 0.09	25

Table 1: Time constants of the averaged time profiles (ATPs)

Note. — Time constants, t_r and t_d (s), of the stretched exponential fit to the averaged pre-peak and post-peak profiles, respectively. Peak fluxes in 64 ms resolution ($\text{ph cm}^{-2} \text{s}^{-1}$) are taken from the BATSE database and are measured in channels 2 and 3. N is the number of bursts in the given brightness interval. For estimation of χ^2 values, see in Appendix B.

Channel #	t_r	t_d	t_d/t_r
1	0.50	0.70	1.40
2	0.42	0.56	1.33
3	0.35	0.42	1.20
4	0.20	0.27	1.35
1 - 4	0.39	0.53	1.35

Table 2: Time constants measured with $\nu = 1/3$ in different energy channels

Note. — Time constants, t_r and t_d , of the averaged time profiles are given for the 280 brightest events in separate energy channels. The value of the index ν was fixed at $1/3$. Relative errors for t_r and t_d are 12%, for t_d/t_r they are 8%.

#	Peak flux	N	ν_r	ν_d
1+2	3 – 200	366	0.338 ± 0.027	0.322 ± 0.026
3+4	1 – 3	597	0.316 ± 0.020	0.359 ± 0.023
5+6	0 – 1	347	0.252^*	0.411 ± 0.034
All	0-200	1310	0.300 ± 0.017	0.371 ± 0.021

Table 3: SE indices for three wide brightness groups

Note. — ν_r , ν_d are best fit SE indices for the 3-parametric (free $\beta, \nu_{r,d}, t_{r,d}$) fit in the $0.5 < t^{1/3} < 6$ interval.
^{*} For sample 5+6, the fit was done in the $1 < t^{1/3} < 6$ time interval because of too strong ATP deformations within 1 second. Errors were not estimated.

Peak counts	t_r	t_d	Trigger efficiency
Parent sample	0.32	0.43	1.00
250	0.31	0.42	0.97
150	0.31	0.42	0.83
110	0.32	0.44	0.71
75	0.33	0.47	0.57

Table 4: Time constants measured with $\nu = 1/3$ for different peak count rate

Note. — Test for robustness of ATP slopes against brightness dependent effects. The parent sample consists of 353 GRBs with the peak count rate in the interval $500 - \infty$. Then it was rescaled to the count rates displayed in the first column. Note that all time constants are correlated as all of them have the same parent sample. Therefore the errors of Table 1 are not applicable here and the time constants for different peak count rates have small dispersion. For association of this table with Table 1 one can use the approximate coefficient 0.0072 to translate peak count rates into peak fluxes with units $\text{ph s}^{-1} \text{cm}^{-2}$.

Fitting interval	$\sigma(t_{r,d})/t_{r,d}\sqrt{N/100}$
$0.125 < t < 8$	0.252
$0.125 < t < 27$	0.219
$0.125 < t < 64$	0.205
$0.125 < t < 125$	0.201

Table 5: Accuracy of the determination of the time constants with fixed SE index ν

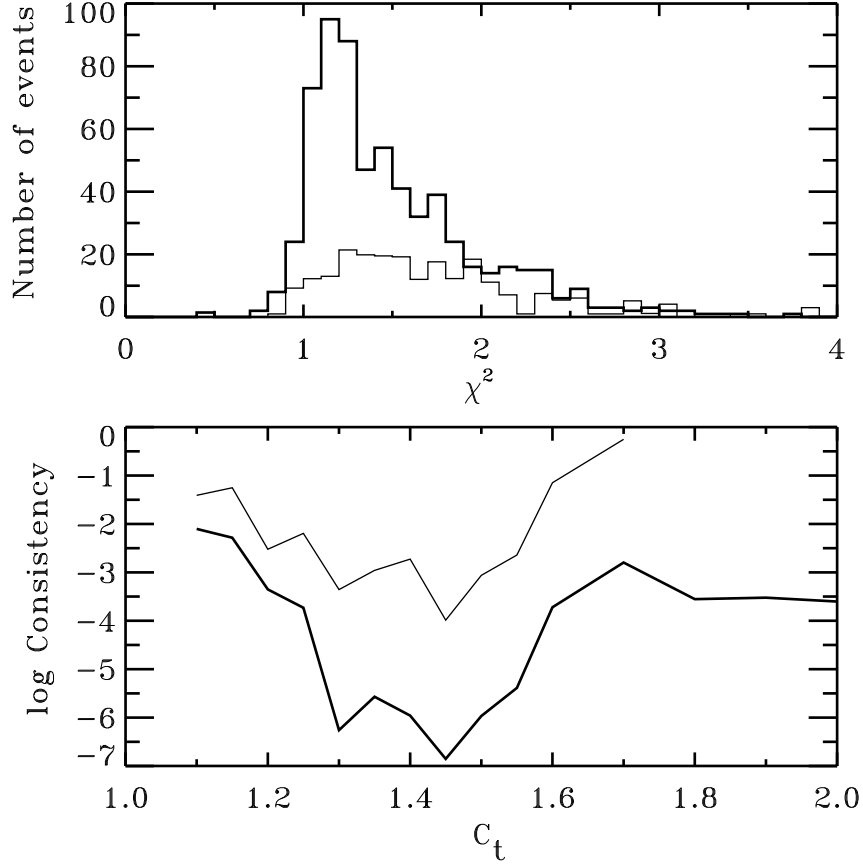


Fig. 1.— a) The reduced χ^2 distribution for “resolved” events with $t_r + t_d > 2$ s. Thick histogram: GRBs with faster rise than decay ($t_r < t_d$), thin histogram: GRBs with slower rise than decay ($t_r > t_d$). b) The consistency level using the Kolmogorov-Smirnov criterion for peak count rate distributions of simple ($\chi_m^2 < C_t$) and complex ($\chi_m^2 > C_t$) GRBs as a function of the χ_m^2 threshold C_t . Thick curve: the condition $t_r < t_d$ is applied when distinguishing simple and complex events, thin curve: the condition is ignored.

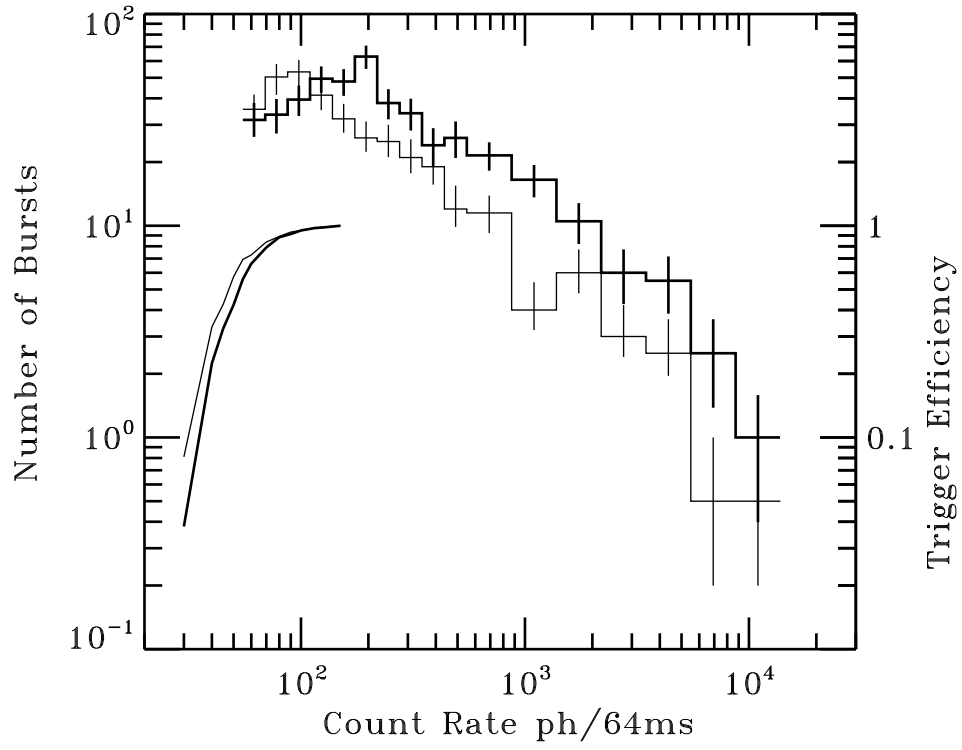


Fig. 2.— Differential peak count rate distributions for simple (thin histogram) and complex GRBs (thick histogram) corrected for the trigger efficiency. The trigger efficiency for simple (thin curve) and complex (thick curve) bursts are plotted in the lower left corner.

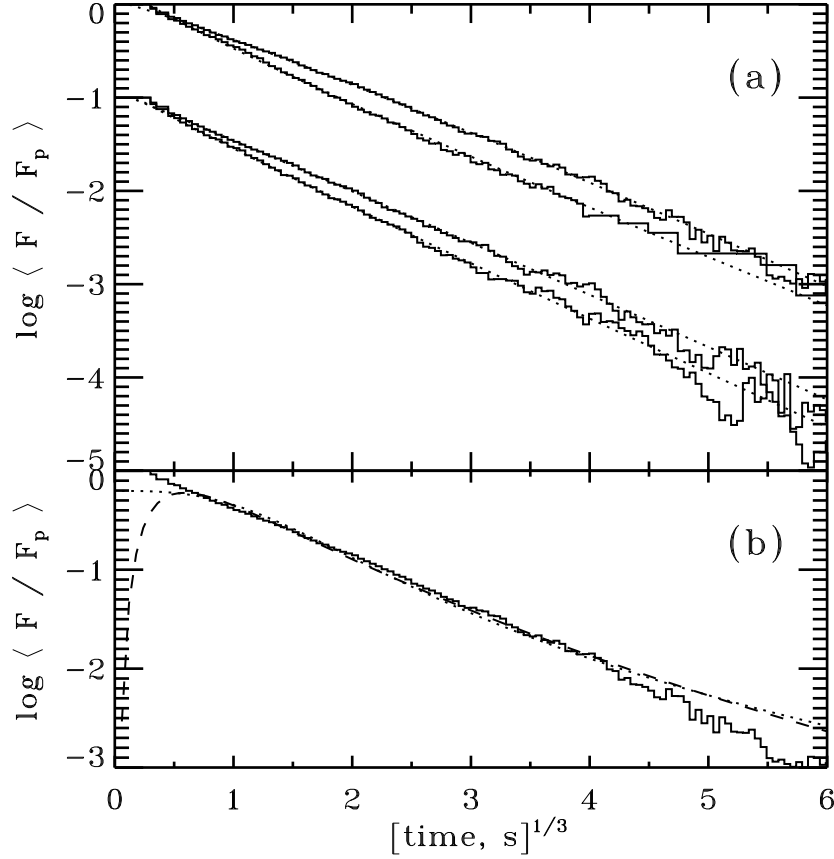


Fig. 3.— a) Rising and decaying slopes of the ATP with their stretched exponential fits. Upper set of curves: the full useful sample, 1310 GRBs; lower set of curves (shifted down for clarity): the 953 brightest GRBs. Rising slopes are steeper than the decaying for both cases. Dotted lines represent the best 3-parametric (β, ν, t_0) stretched exponential fit. Best fit values of ν for the whole sample are 0.30, 0.37 for the rising and decaying slopes, respectively. For the bright sample, $\nu \approx 0.33$, for both slopes. b) Examples of ATP fits with other functions. Dashed curve: parametrization of Mitrofanov et al. (1997) $F(t) = \beta[t_0/(t_0 + t)]^\alpha$; dotted curve: the one-sided log-normal distribution (see text)

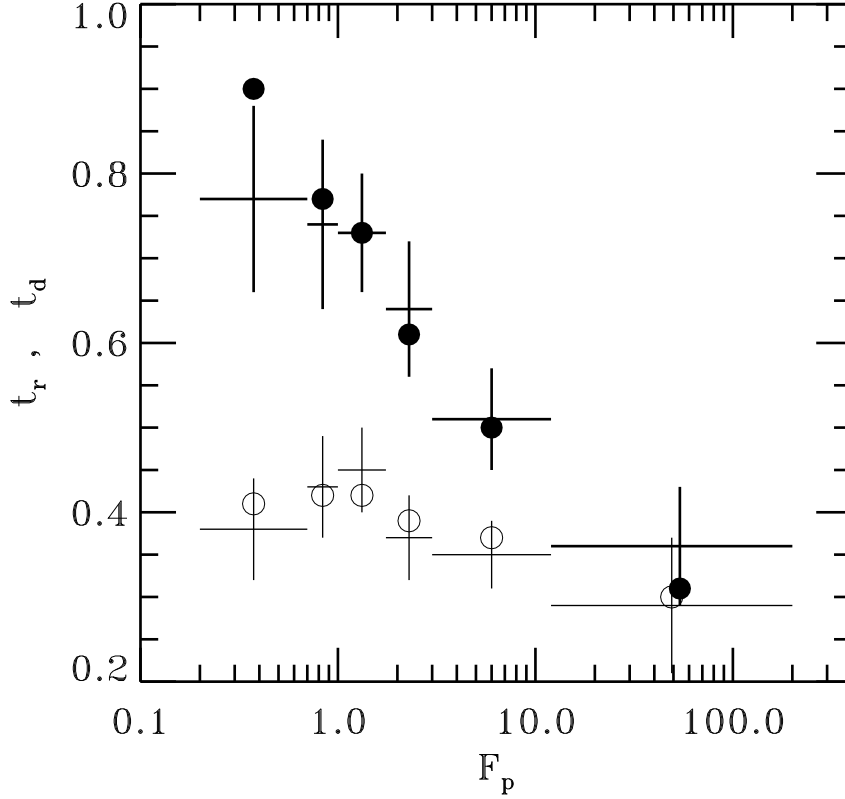


Fig. 4.— Time constants, $t_{r,d}$, vs peak photon flux in 64 ms time resolution, F_p (ph cm $^{-2}$ s $^{-1}$). The SE index, ν , was fixed to 1/3. Upper and lower crosses represent results for the post-peak (decaying) and pre-peak (rising) ATPs, respectively. Error bars in $t_{r,d}$ correspond to values in Table 5, Appendix B. Error bars in photon flux represent the width of the brightness group. Open and filled circles represent best fit values for $t_{r,d}$ with ν fixed at 0.30 and 0.37 and rescaled with the factors 1/0.51 and 1/1.6 for the rising and decaying slopes, respectively.

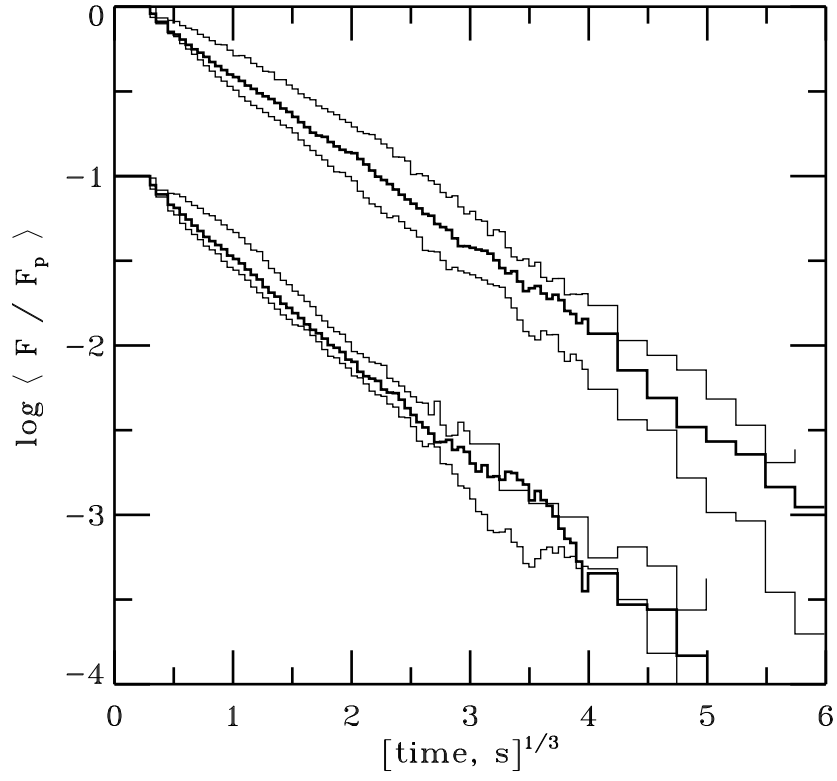


Fig. 5.— Decaying and rising slopes of the ATP for different brightness groups: strong (samples 1+2), medium (samples 3+4), and weak (samples 5+6). Rising slopes are shifted down for clarity. Stronger bursts have smaller time constants (slopes are sharper).

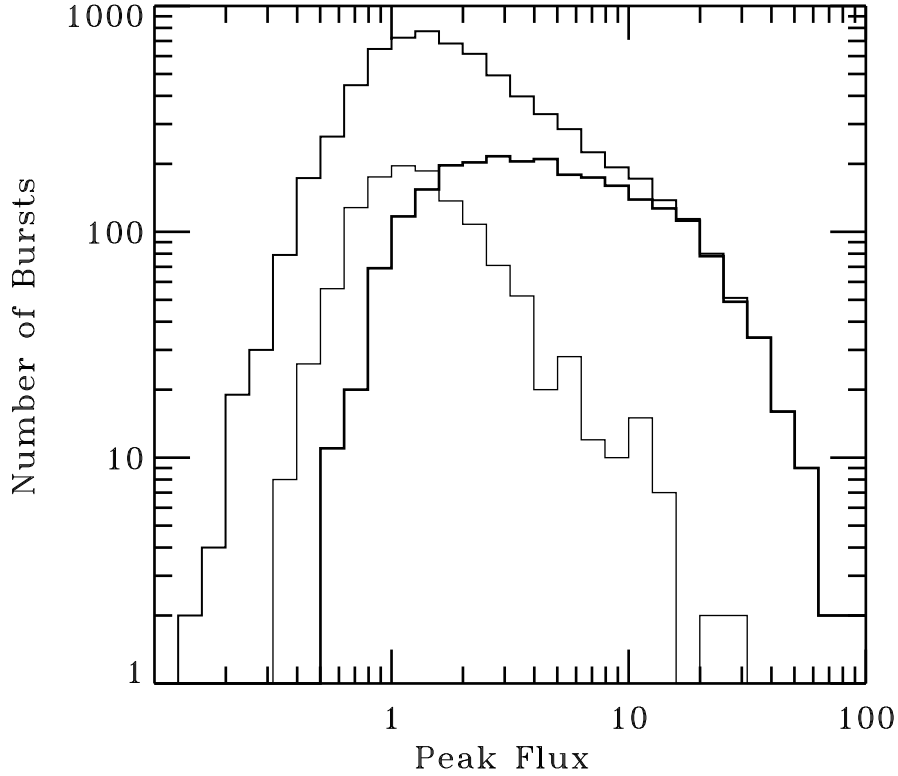


Fig. 6.— Example of intrinsic peak luminosity function for events simulated with the pulse avalanche model (upper curve). The peak amplitudes of individual pulses were sampled with a log-normal distribution, $dn/dp \sim \exp[-\log^2 p/2\sigma^2]$ with $\sigma = 0.7$. Lower curves are peak distributions for simple (thin histogram) and complex (thick histogram). The separation of simple and complex events was obtained using the same procedure as described in § 3.1 rescaling simulated bursts to the same peak count rate 55 counts/64 ms. The χ^2 distribution for simulated events is more sharply peaked at $\chi^2 \sim 1$ than was the case for real events.

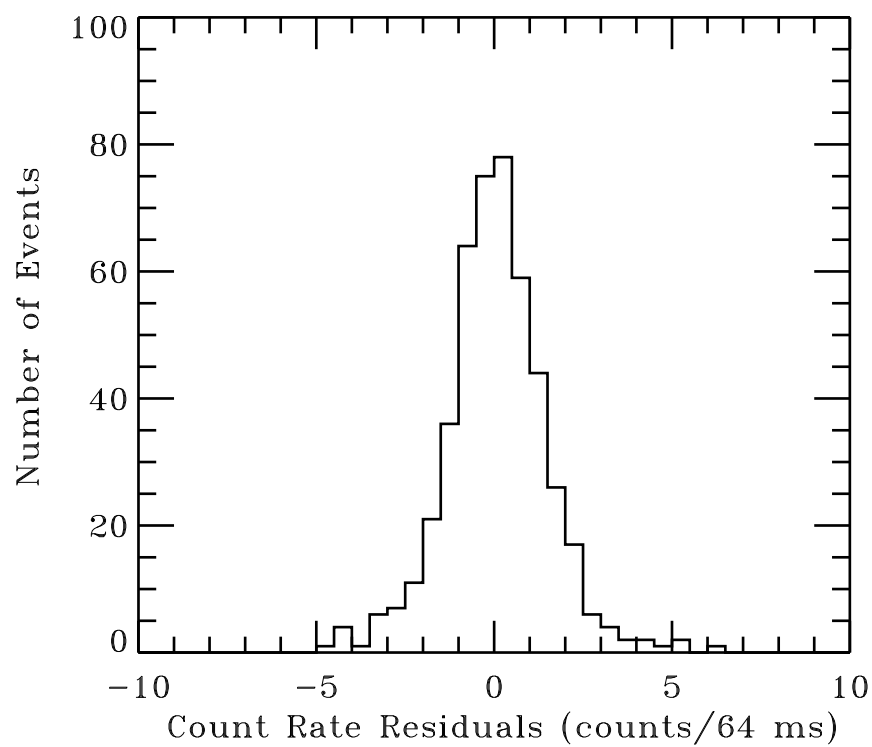


Fig. 7.— Residuals to background fits in “observational windows” in time intervals where the contribution of the GRB is invisible.

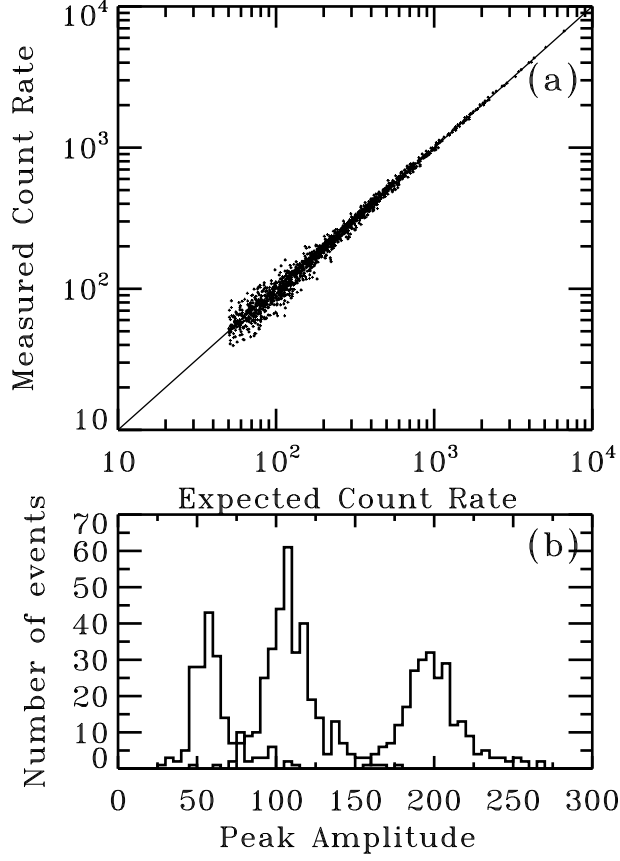


Fig. 8.— Test of the procedure for the peak count rate estimate. a) expected vs. measured count rate scattering plot obtained with bright events longer than 2 s rescaled to lower brightness. Note that the peak count rate estimate is based on the 64 ms resolution. b) Distributions of the measured peak count rates at fixed expected count rate P_p : $P_p = 55$ counts/64 ms; $P_p = 110$ counts/64 ms; $P_p = 200$ counts/64 ms. Bursts which did not pass the simulated trigger are not included. For description of rescaling and triggering procedures, see § A.3.

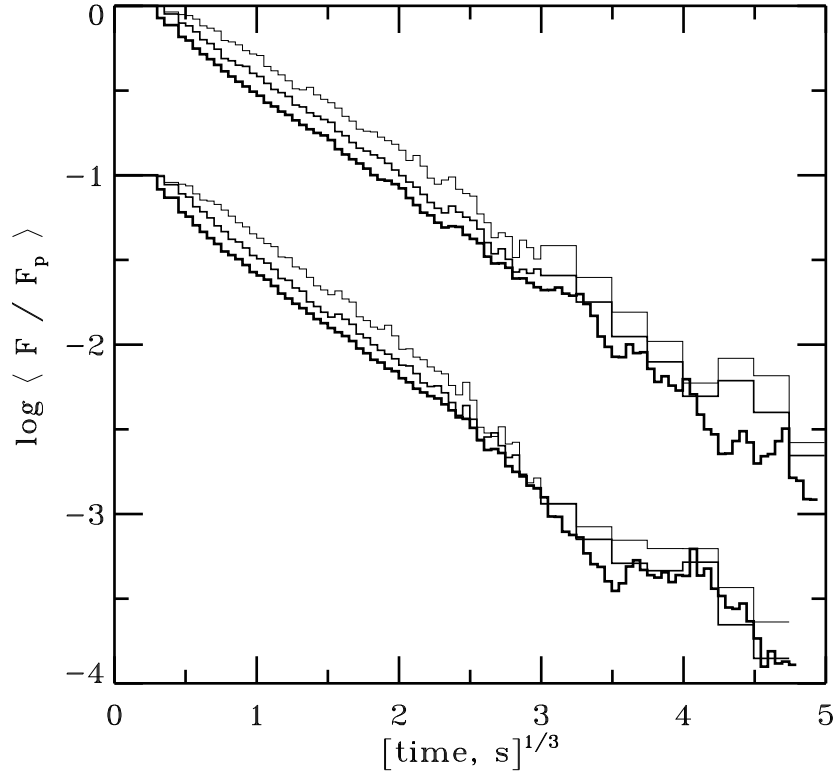


Fig. 9.— Deformations of the decaying (upper histograms) and rising (lower histograms) slopes of ATP after rescaling of the parent sample of bright bursts. Thickness of the histogram decreases from the parent sample to peak count rate 150 counts/64 ms and to peak count rate 75 counts/64 ms. The ATP for 250 counts/64 ms is almost indistinguishable from the parent sample.

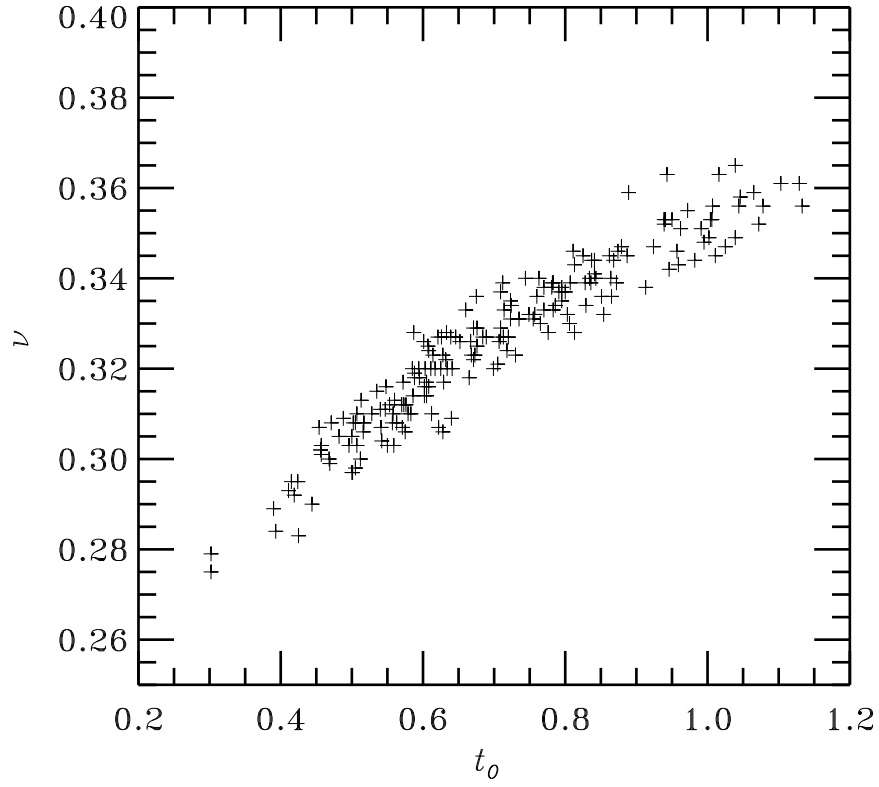


Fig. 10.— Scattering plot for best fit values of ν and t_0 for a pulse avalanche simulations.

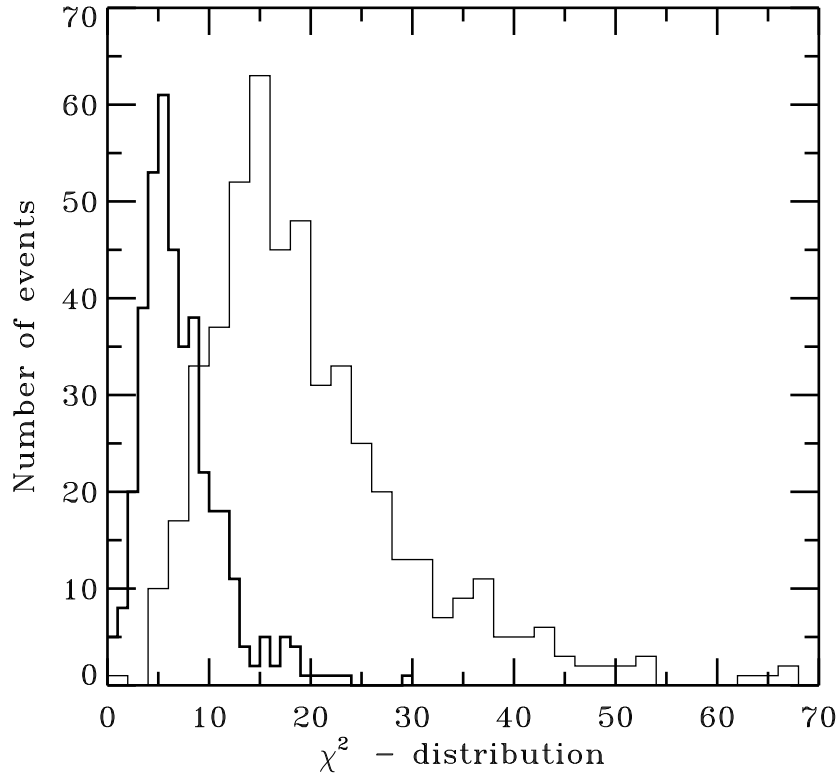


Fig. 11.— Examples of χ^2 distributions for simulated samples of GRBs. Thick histogram: 3-parametric fit of the decaying slope (free β, ν , and t_0), 1000 events in the sample, 15 formal degrees of freedom; thin histogram: 3-parametric simultaneous fit of both slopes of the ATP (free t_r, t_d , and a common β ; ν is fixed to $1/3$), 300 events in the sample, 33 formal degrees of freedom.